Academia
Earth and Planetary Science

10.20935/AcadEPS8589

Research Article

# Tetrahedrite-group minerals record hydrothermal fluid evolution in Southern Kamchatka

Elena D. Skilskaya[1,*], Ksenia O. Shishkanova[1], Daria A. Yablokova[1], Vladimir V. Kozlov[1], Ilya V. Vikentyev[2], Vladimir A. Lebedev[2], Olga R. Rozhko[1]

[1] Institute of Volcanology and Seismology, Far East Branch of the Russian Academy of Sciences, Petropavlovsk-Kamchatsky, Russia

[2] Institute of Geology of Ore Deposits, Petrography, Mineralogy and Geochemistry, Russian Academy of Sciences, Moscow, Russia

* Correspondence: wideworldscience@gmail.com

**Received:** 10 August 2026 | **Accepted:** 8 October 2026 | **Published:** 28 October 2026

## Abstract

**Introduction:** The Vilyuchinskoe gold–silver (Au-Ag) ore occurrence (Southern Kamchatka) is spatially associated with the Rodnikovoe paleovolcano and hosted by Oligocene andesite–dacite tuffs and lava flows intruded by gabbro–diorite. This study aims to reconstruct the physicochemical evolution and timing of ore formation using tetrahedrite-group minerals, fluid inclusions and potassium-argon (K-Ar) geochronology.

**Materials and methods:** The chemical compositions of ore minerals were analyzed using scanning electron microscopy coupled with energy dispersive X-ray spectroscopy (SEM-EDS). Fluid inclusion microthermometry was performed on vein quartz using a Linkam THMSG 600 heating–freezing stage. K-Ar dating was carried out on adularia and adularia–quartz fractions.

**Results:** Three new dates obtained from vein adularia yield ages of 4.8 ± 0.3 Ma, 1.49 ± 0.19 Ma and 1.18 ± 0.18 Ma. The tetrahedrite-group minerals were formed in three stages. Stage I consists of fahlore-I (tennantite and tetrahedrite), pyrite, sphalerite (FeS 1.51 mol.%) and minor chalcopyrite. Stage II is represented by fahlore-II (tennantite and tetrahedrite) replacing chalcopyrite, associated with sphalerite (FeS 8.32 mol.%) and galena. Fahlore-II shows elevated Ag (up to 7.84 wt.%) and Bi (up to 5.11 wt.%). Stage III comprises tellurides, selenides, and fahlore-III (tellurium-bearing fahlore and goldfieldites). Fluid inclusion data were as follows: Stages I–II—236–277 °C (1.6–2.6 wt.% NaCl eq.); Stage III—210–249 °C (0.5–1.7 wt.% NaCl eq.).

**Conclusions:** New geochronological data obtained in this study indicate that the Vilyuchinskoe ore occurrence formed during at least two distinct pulses of hydrothermal activity, corresponding to the Pliocene (~5 Ma) and Early Pleistocene (~1.3 Ma). The mineralogical study, together with fluid inclusion data, indicates that fahlores were deposited from hydrothermal fluids at 210–277 °C under decreasing sulfur fugacity and increasing tellurium activity due to fluid cooling $fTe_2$. The Vilyuchinskoe ore occurrence is classified as a transitional subepithermal intermediate-sulfidation system, contributing to the understanding of such systems and to prospecting in Southern Kamchatka and other regions.

**Keywords**: tennantite; tetrahedrite; tellurides; selenides; Vilyuchinskoe; Kamchatka

# 1. Introduction

One of the most precise indicators of ore genesis is the tennantite–tetrahedrite series of minerals (also called fahlore), which represents one of the most widespread and economically significant groups of sulfosalt minerals, occurring in diverse ore deposits worldwide [1–6]. These minerals form a continuous isomorphic series between two end-members: tennantite ($Cu_{12}As_4S_{13}$) and tetrahedrite ($Cu_{12}Sb_4S_{13}$) [7–9]. The wide compositional variations in fahlore-group minerals serve as indicators of physicochemical conditions of ore formation, enabling the reconstruction of temperature, pressure, sulfur fugacity, and volatile component contents during deposit formation.

The presence of fahlore-group minerals in the ores of the Kamchatka gold–silver epithermal deposits has been reported in several publications [10–15]. The most diverse assemblages, characterized by a large number of intraspecific varieties distinguished by the ratios of As, Sb, Cu, Ag, Zn, Hg, Fe, as well as the contents of trace elements (Se, Te, Bi, In), are typical of ores of the Ozernovskoe high-sulfidation gold deposit in Central Kamchatka [13].

The Vilyuchinskoe gold–silver ore occurrence is situated within the Southern Kamchatka mining district, which encompasses three epithermal gold–silver deposits (Rodnikovoe, Mutnovskoe, and Asachinskoe), over 30 gold–silver ore occurrences, as well as geothermal systems and hydrothermal spring fields. At present, the Asachinsky Mining and Processing Plant is the only operating mining enterprise in the Southern Kamchatka mining district, located several kilometers to the south of the Vilyuchinskoe ore occurrence. The bulk of exploration work at the Vilyuchinskoe ore occurrence was carried out between 1976 and 1991. The length of the veins is 260–1300 m. The gold grades show considerable variation, up to 48–57 g/t in bonanza zones. The average gold content is 12.2 g/t. Silver concentrations are likewise highly variable, ranging from tens to 945 g/t, with a mean of 102 g/t [16]. Despite significant interest in the Vilyuchinskoe ore occurrence as a promising site, its geological structure, ore composition, and formation conditions remain insufficiently studied. To date, only a few brief mentions of the Vilyuchinskoe mineralogy exist in the literature [12, 15], and no systematic investigation has been undertaken to constrain the formation conditions of this epithermal system and compare it with the epithermal gold deposits in other regions. In this paper we present new results on fahlore mineralogy, age dating and fluid inclusion studies, along with a discussion of the conditions controlling fahlore chemistry and its link to precious metal deposition. This study provides new insights into the nature and genesis of these deposits, and offers a basis for their comparison with other epithermal precious-metal deposits.

## 1.1. Geology of the study area

The Vilyuchinskoe ore occurrence, along with the Rodnikovoe epithermal gold–silver deposit, constitutes the Rodnikovoe ore field. This field is confined to the Rodnikovoe paleovolcano in Southern Kamchatka, which is one of the most highly volcanically and seismically active regions in the Kuril–Kamchatka volcanic arc (**Figure 1**). The Vilyuchinskoe ore occurrence covers an area of 6.3 $km^2$ and is localized in the northwestern part of the Rodnikovoe ore field, 4 km northwest of the Rodnikovoe gold–silver deposit (**Figure 1**). The geology of the Vilyuchinskoe ore occurrence is represented by Oligocene–Miocene volcanic rocks of the Paratunskaya Formation, Miocene gabbro–diorite intrusions, Pliocene subvolcanic bodies of rhyolitic and andesitic composition, Pliocene volcanic rocks of the Alneiskaya Formation, and Quaternary mainly volcanic series.

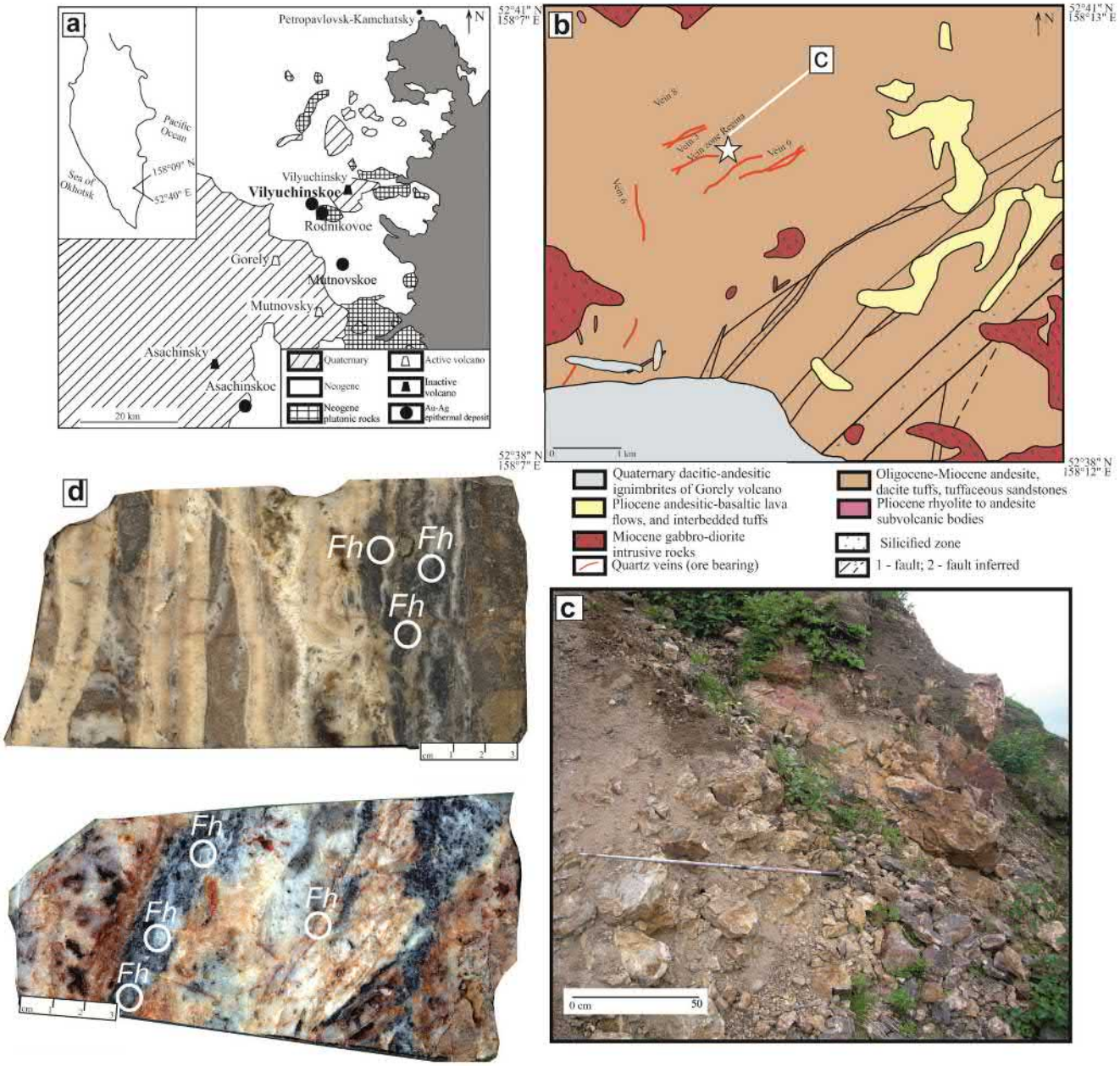



**Figure 1.** The location (modified after [17]) and schematic geological map (modified after [18]) of the Vilyuchinskoe gold–silver ore occurrence: (**a**) location map of Southern Kamchatka showing the distribution of active and inactive volcanoes, neogene and quaternary rocks, and epithermal gold deposits; (**b**) detailed geological map of the study area, the star symbol indicates the main ore-bearing zone; (**c**) outcrops of the Regina vein zone; (**d**) representative samples of ores containing visible disseminated fahlore (Fh), the white circles marked "Fh" indicate sampling points for fahlore.

The Paratunskaya Formation, which occupies 80% of the site area, consists of andesite–dacite tuffs that pass upward in the section into andesite–dacite and andesite flows with interbeds of tuffs of the Alneiskaya Formation. The rocks of the Paratunskaya Formation are intruded by gabbro–diorite subvolcanic intrusions and dikes of andesite and dacite composition. Pliocene subvolcanic andesite bodies are not related to ore mineralization and have a limited distribution.

The Quaternary volcanic series at the ore occurrence are represented by a cover of a sheet-like ignimbrite body of the Gorely volcano, which overlies the earlier volcanic units in the south (**Figure 1**). Hydrothermal alterations are represented by micaceous-quartz metasomatic rocks, monoquartzites, argillic metasomatites, and silicified volcanic rocks. The ores are of the classic hydrothermal gold–silver mineral type and are represented by quartz-carbonate-adularia veins with an uneven distribution of ore minerals [16]. They typically contain minor concentrations of Cu, As, Zn, and Pb, which reach maximum values in orebodies enriched in sulfosalts [12]. Within the ore occurrence, the Vilyuchinskoe ore-bearing zone extends for 3 km with a width of about 500 m. The most promising targets for further study and economic potential assessment are the Regina vein zone, ranging from 5 to 30 m in thickness and about 2 km in length, and Vein No. 9, which is spatially associated with the Regina zone [16]. The Vilyuchinskoe ore occurrence, similar to other hydrothermal gold–silver–polymetallic deposits in Southern Kamchatka, is characterized by a considerable diversity of ore textures. Disseminated textures are dominant, but brecciated and breccia-like textures are also widely represented. Particularly striking are banded, colloform-banded and cockade textures, which are among the most distinctive features of the mineralization.

## 2. Materials and methods

A total of 30 samples were collected from the central part of the Regina vein zone and Vein No. 9 of the Vilyuchinskoe ore occurrence during field work (**Figure 1**). The samples include 40 polished thick sections and eight doubly polished plates for fluid-inclusion analysis.

Mineral assemblages were studied using Axioskop 40 (Carl Zeiss, Oberkochen, Germany) and Eclipse LV 100 pol (Nikon, Shinagawa City, Japan) microscopes equipped with digital cameras at the Laboratory of Volcanogenic Ore Formation of the Institute of Volcanology and Seismology (IVS), Far East Branch, Russian Academy of Sciences (RAS) (Petropavlovsk-Kamchatsky) within a research topic FWME-2024-0006 «The Role of Hydrothermal Systems of the Kuril-Kamchatka Volcanic Arc in the Redistribution of Mantle and Crustal Matter in Processes of Mineral Ore Genesis». The chemical composition and textural features were analyzed using scanning electron microscopy on a Vega III Tescan instrument (Brno, Czech Republic) equipped with an X-Max 80 energy-dispersive detector and Wave 500 wave-dispersive detector (Oxford Instruments, High Wycombe, UK) at the Shared Research Facility «Kamchatka Center for Elemental, Mineral, and Isotope Analysis» of IVS Far East Branch, RAS (Petropavlovsk-Kamchatsky). Measurements were performed under high vacuum ($0.9–2.9 \times 10^{-5}$ mbar), at an accelerating voltage of 20 kV and a beam current of 1 nA. Representative spectra with total counts of 2–5 million were used for samples and standards. AZtec Oxford Instruments software, version 3.1, was used for detailed analysis of mineral textures and compositions. The following substances were used as standards: pure elements Bi, Mn, In, Se; an Au-Ag alloy; and the minerals pyrite, chalcopyrite, sphalerite, greenockite, antimonite, and auripigment. The chemical composition of minerals was determined by exciting atoms of chemical elements with a finely focused electron beam (3.0–5.0 μm).

Fluid inclusion microthermometry was carried out in vein quartz using a Linkam THMSG 600 heating–freezing stage (Linkam Scientific Instruments, Redhill, UK) coupled with a Nikon optical microscope (Nikon, Japan). The measurement accuracy was ±5 °C for low-temperature measurements and ±0.1 °C for homogenization temperatures. The stage operates in the temperature range from −195 to +600 °C. Heating rates were 0.1 °C/min for ice melting and 1 °C/min for homogenization. The final ice-melting and homogenization temperatures were recorded. The salinity was calculated from final ice-melting temperatures using [19]. Measurements were performed at the Laboratory of Volcanogenic Ore Formation, Institute of Volcanology and Seismology and Vitus Bering Kamchatka State University (Petropavlovsk-Kamchatsky, Russia).

The radiogenic argon content was determined using the potassium-argon (K-Ar) method with an MI-1201 IG mass spectrometer («Electron» plant, Sumy, Ukraine) employing isotope dilution with $^{38}Ar$ as a tracer; K was determined using flame spectrophotometry at the Institute of Geology of Ore Deposits, Petrography, Mineralogy and Geochemistry, Russian Academy of Sciences (Moscow). When calculating the age, the following constants were used: $\lambda_K = 0.581 \times 10^{-10}$ year$^{-1}$, $\lambda_\beta = 4.962 \times 10^{-10}$ year$^{-1}$, and $^{40}K = 0.01167$ (at.%). Ages are reported with $2\sigma$ analytical uncertainty.

## 3. Results

### 3.1. K-Ar geochronology

In this study, three K-Ar age determinations were performed on vein minerals from the Vilyuchinskoe occurrence. For two monomineralic adularia fractions (K = 1.07 wt.%, $^{40}Ar_{rad}$ = 0.11 ng/g and K = 2.17 wt.%, $^{40}Ar_{rad}$ = 0.178 ng/g), the calculated ages were 1.49 $\pm$ 0.19 and 1.18 $\pm$ 0.18 Ma, respectively (**Table S1**). The adularia-quartz mixture, characterized by a higher potassium content (K = 1.57 wt.%) and an elevated concentration of radiogenic argon (0.520 ng/g), yields an age of 4.8 $\pm$ 0.3 Ma.

### 3.2. Vein mineralogy

Quartz is the most common vein mineral in the Vilyuchinskoe ore occurrence. Several varieties have been preliminarily distinguished based on color and internal texture. Cryptocrystalline quartz is the most widespread, typically occurring as amorphous aggregates with metacolloidal textures probably inherited from silica gel. Another variety exhibits fine-grained and allotriomorphic textures, with grain sizes generally ranging from 0.5 to 1.5 mm. Its color varies from light gray (transparent) to yellowish. Both varieties are closely associated and are classified as productive quartz, which constitutes the main mass of the orebodies. This quartz hosts virtually all ore minerals, ranging from sulfides to native gold, as well as gangue minerals such as adularia and, more rarely, carbonates.

### 3.3. Ore mineralogy

Based on the observed intergrowth relationships of quartz with ore minerals, three mineral stages are recognized.

Pyrite is the most abundant ore mineral, showing a diversity of morphological forms and sizes (**Figure 2**). It was observed as individual grains, elongated clusters of finer subhedral crystals, inclusions and intergrowths with other ore minerals. Disseminated pyrite grains range widely in size, from 0.1–0.2 mm to 3–5 mm and have commonly idiomorphic shapes. It is closely associated with sphalerite and chalcopyrite. Inclusions of pyrite were commonly found in chalcopyrite, which is overprinted by late tennantite-tetrahedrite-series minerals and in some rare cases in sphalerite. The scanning electron microscopy coupled with energy dispersive X-ray spectroscopy (SEM-EDS) data show impurity-free pyrite and pyrite containing impurities of As, Pb, Bi, Cu and Sb. However, impurities of As are very common and have a higher concentration (up to 5.52 wt.%) than others. The As-rich zones are frequently marked by growth zones of pyrite, but in some cases the core of pyrite is enriched in As, while the rest of the grain does not contain As (**Figure 3a–c**). Impurities of Pb, Cu, Bi, and Sb are less common, with contents of 3.85, 1.51, 0.21 and 2.62 wt.%, respectively (**Table S2**).

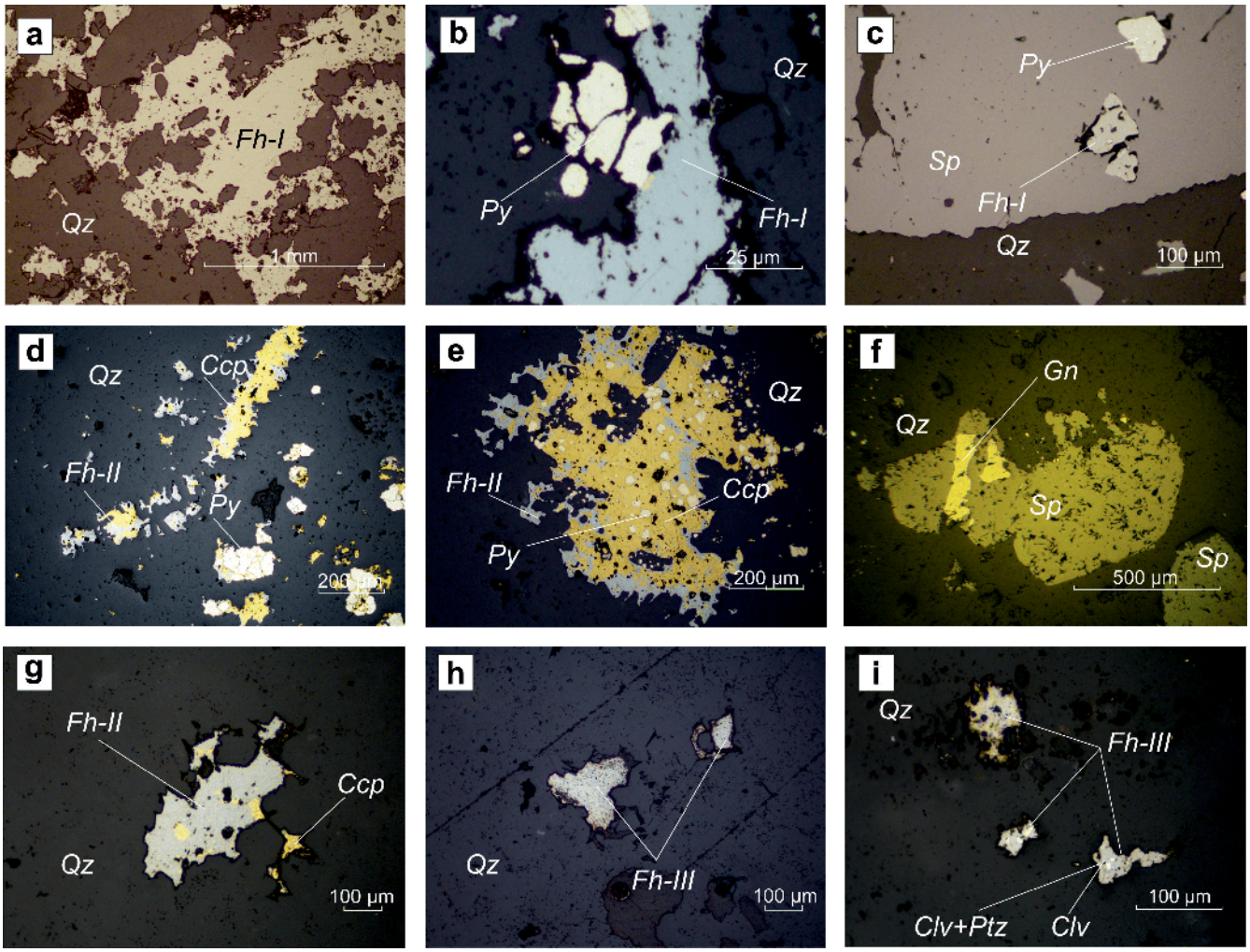



**Figure 2.** Photomicrographs of ore minerals under reflected light: (**a**) coarse grains of fahlore-I (Fh-I); (**b**) fahlore-I (Fh-I) intergrown with early pyrite; (**c**) inclusions of fahlore-I (Fh-I) and pyrite in sphalerite; (**d**) interstices of fahlore-II (Fh-II) around grains of pyrite and chalcopyrite; (**e**) fahlore-II (Fh-II) overgrowing early chalcopyrite that contains pyrite inclusions; (**f**) intergrowth of sphalerite with galena; (**g**) fahlore-II (Fh-II) replacing chalcopyrite; (**h**) fahlore-III (Fh-III) in quartz; (**i**) fine grains of fahlore-III (Fh-III) in association with tellurides (calaverite, petzite - Clv+Ptz). Fh: fahlore, Py: pyrite, Sp: sphalerite, Gn: galena, Ccp: chalcopyrite, Clv: calaverite, Ptz: petzite, Qz: quartz.

Sphalerite is the second most abundant sulfide mineral in the ore of the Vilyuchinskoe Au-Ag occurrence. It occurs as individual grains of diverse size and morphology, and as massive aggregates. The individual sphalerite grains range in size from 0.05–0.50 mm to 2–3 mm, with finer grains predominating. Coarse anhedral grains are commonly found in intergrowths with galena and pyrite. Fine-grained sphalerite is associated with chalcopyrite, tennantite, tetrahedrite and pyrite (**Figure 2, Figure 3d**). Some sphalerite grains contain emulsion blebs of chalcopyrite and, much less commonly, galena and fahlore. Tiny galena veins are filled fractures in sphalerite (**Figure 3e**).

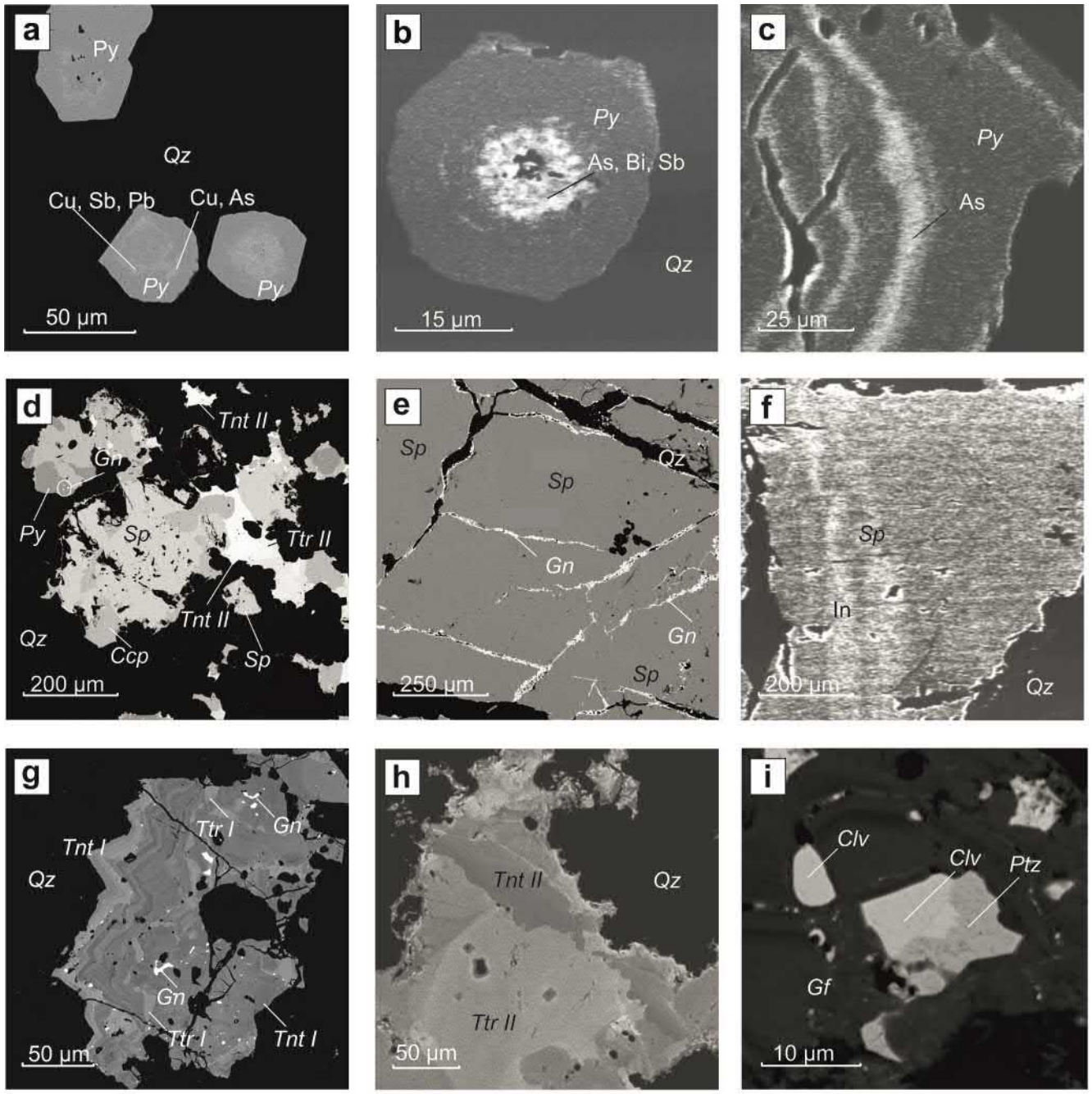



**Figure 3.** SEM-BSE images of ore minerals: (**a**) zonal pyrite with respect to As, Cu, Pb, Sb; (**b**) idiomorphic pyrite crystal with a core composed of compounds containing As, Bi, Sb; (**c**) pyrite with As growth zoning; (**d**) modes of occurrence of sphalerite; (**e**) sphalerite crystal with fractures filled by galena; (**f**) In-rich zone in sphalerite; (**g**) varieties of occurrence forms of tetrahedrite-group minerals and characteristics of their internal structure (Stage I); (**h**) Stage II tetrahedrite-group minerals (tennantite-II and tetrahedrite-II); (**i**) calaverite and petzite in association with goldfieldite. Py: pyrite, Sp: sphalerite, Ccp: chalcopyrite, Gn: galena, Tnt: tennantite, Ttr: tetrahedrite, Gf: goldfieldite, Clv: calaverite, Ptz: petzite, Qz: quartz. SEM-BSE: scanning electron microscopy-backscattered electron imaging. Roman numerals I and II designate mineralization stages (Stage I and Stage II).

Sphalerite (approximately 90 analyses using SEM-EDS) contains the following impurities: Fe 0.00–4.68 wt.%, Cd 0.00–6.32 wt.%, Mn 0.00–0.19 wt.%, Cu 0.00–2.32 wt.%, and In 0.00–3.24 wt.% (**Table S2**). Very small quantities

of Ag and Sb were also detected. Based on Fe content, sphalerite is divided into an Fe-free category, namely cleiophane [12, 20], and a low-Fe category with Fe of 0.20–4.68 wt.% (**Table S2**). Indium forms the In-rich zones in sphalerite grains (**Figure 3f**). The Fe- and Cd-bearing sphalerite exhibits no compositional zoning linked to localized Fe and Cd enrichment. The presence of minor amounts of Cu, Ag, and Sb in sphalerite can be attributed to isomorphic substitution and/or the presence of micro-inclusions of chalcopyrite and fahlore.

Galena occurs as isolated, commonly cataclastic, grains with near-idiomorphic outlines. It also forms intergrowths with sphalerite, and, less commonly, with pyrite. Veinlets of galena cutting through sphalerite were also observed. Grain size is about 1–2 mm.

Chalcopyrite is present almost ubiquitously. It occurs as individual fine anhedral grains, nests, veinlets, and intergrowths with pyrite, fahlore minerals, and sphalerite (**Figure 2d,e**). Chalcopyrite was also observed as blebs within sphalerite grains. Grain sizes range from 0.2–0.5 to 2–3 mm. Occasionally, it cements cataclastic grains of earlier precipitated pyrite. It is also observed as inclusions within fahlore-group minerals.

Greenockite is a rare mineral at the ore occurrence. It most commonly fills microfractures in Cd-bearing sphalerite or forms collomorphic rims around sphalerite in association with galena and pyrite. Greenockite contains an impurity element Zn, whose concentration reaches 8.87 wt.% (**Table S2**).

Bornite is relatively rare. It occurs as irregular anhedral grains up to 40–50 μm in size and forms complex intergrowths with fahlore and pyrite.

Acanthite with size ranging from 50 to 100 μm is rarely observed infilling voids within the quartz.

Antimonite (stibnite) was encountered in trace amounts within the mass of oxidized minerals containing Sb, Ag, and As. Impurities of Cu and As were detected in the antimonite. A distinctive feature of its aggregates is the presence of rims composed of complex oxides.

A stromeyerite-type mineral was identified for the first time at the ore occurrence, occurring as an anhedral grain up to 15 μm in size in intergrowth with Sb-bearing oxides.

### 3.3.1. Tellurides

Calaverite and petzite are the only Au-Ag tellurides found in this study. They form intergrowths and occur as inclusions 10–20 μm in size within goldfieldite, arsenogoldfieldite and stibiogoldfieldite.

Coloradoite is relatively rare, occurring as xenomorphic grains scattered in the quartz matrix. Grain sizes range from 2–3 μm to 15–20 μm. The chemical composition of tellurides is presented in **Table S3**.

### 3.3.2. Selenides

Naumannite is found primarily as small inclusions, generally no larger than 5 μm in size, within goldfieldite. Clausthalite occurs in intergrowths with petzite and forms inclusions approximately 10 μm in size within tellurian fahlore.

### 3.3.3. Sulfosalts

Enargite occurs in close intergrowths with chalcopyrite. It is characterized by anhedral forms with grain sizes of 10–15 μm.

### 3.3.4. Tetrahedrite-group minerals

The early-generation fahlore is represented by fahlore-I (Stage I) and fahlore-II (Stage II) (**Figure 2**).

Fahlore-I comprises large weakly zoned to unzoned tennantite grains and strongly zoned tennantite–tetrahedrite grains. Some unzoned tennantite-I grains occur in association with coarse pyrite and sphalerite. Tennantite-I is characterized by a Cu content of 9.80–12.18 atoms per formula unit (apfu), predominance of Zn over Fe, positive correlation between Ag and Sb, and presence of Mn (up to 0.43 wt.%). In some grains, Ag (up to 0.16 apfu), Te (up to 0.02 apfu), Bi (up to 0.04 apfu), Se (up to 0.05 apfu), and In (up to 0.30 apfu) were detected (**Table S4**). The In concentration is strictly limited to tennantite-I, ranging from 1.34 to 2.26 wt.% (up to ~0.30 apfu). In-bearing tennantite has Cu up to ~12.18 apfu, Ag ≤ 0.09 wt.%, Zn ≤ 0.08 wt.%, and Fe up to 4.87 wt.% (~1.29 apfu). Indium correlates positively with As and Fe and negatively with Sb, Zn, and Ag. Indium is absent in fahlore of Stage II and Stage III. Bismuth in tennantite-I forms a minor admixture (0.04–0.54 wt.%).

Tetrahedrite-I is characterized by Cu concentration of ≈10.07–10.46 apfu, elevated silver concentrations relative to tennantites, and Zn predominance over Fe (**Table S4**). Zoned grains of tennantite-I and tetrahedrite-I exhibit alternating As-enriched and Sb-enriched zones, with a decrease in the width of As-rich zones from core to rim (**Figure 3g**). This indicates a progressive increase in the antimony proportion in the hydrothermal fluid.

Fahlore-II (Stage II) overgrows chalcopyrite and also develops as thin veinlets cutting sphalerite grains. Fahlore-II is mainly represented by tennantite-II and tetrahedrite-II, which form composite aggregates replacing chalcopyrite and other earlier sulfides (**Figure 2d,g**). Tennantite-II is enriched in Cu up to 10.64 apfu (**Table S4**). The Zn content predominates over Fe. Some tennantite-II shows relatively notable concentrations of Bi (up to 0.03 apfu) and Te (up to 0.06 apfu) (**Table S4**).

Tetrahedrite-II includes Ag in amounts up to 7.84 wt.% (**Table S4**). Tetrahedrite-II containing Ag shows lower Cu concentrations, down to ~8.09 apfu (**Table S4**). In terms of internal structure, such fahlore exhibits a complex mosaic-blocky texture (**Figure 3h**). According to our data, Bi is strongly concentrated in Sb-rich tetrahedrite-II, reaching 2.17–5.11 wt.% (up to ~0.40 apfu) at high Sb (19.79–21.57 wt.%), Ag (1.04–7.84 wt.%), and Zn (5.62–7.31 wt.%) and low As (3.95–8.64 wt.%).

Later-generation fahlore-III (Stage III) occurs as fine grains (up to 50 μm) containing inclusions of Au-Ag tellurides, Ag and Pb selenides, and sulfides. These fahlores are represented by goldfieldite and its varieties (**Figure 3i**, **Table S4**). Tellurium-bearing fahlore shows elevated Cu contents, reaching up to 11.60 apfu in arsenogoldfieldite and 11.07 apfu in stibiogoldfieldite, with a complete absence of Ag. The Te concentrations range from 1.41 apfu in arsenogoldfieldite to 2.33 apfu in stibiogoldfieldite, corresponding to 11.21–18.79 wt.% Te. Se ranges from 1.52 to 3.74 wt.%. Zn is present only in arsenogoldfieldite, with maximum values up to 0.40 apfu. Se is present as a minor element in arsenogoldfieldite (up to 1.01 apfu) and stibiogoldfieldite (1.84 apfu) (**Table S4**). Indium and bismuth are not detected in fahlore-III.

### 3.3.5. Supergene minerals

Supergene minerals are extensively developed and represented by iron oxides and hydroxides, symplesite, copper minerals (chalcocite, covellite, malachite), lead minerals (anglesite, cerussite), and complex iron oxides containing arsenic, antimony and sulfur. Iron oxides and hydroxides typically form rims around sulfides. Their dimensions range within 100 μm. Symplesite occurs as radial-acicular rounded aggregates within the vein matrix. Chalcocite and covellite are observed as rims and irregularly shaped formations along the boundaries

of sphalerite and chalcopyrite. Malachite was encountered as a single grain. Anglesite and cerussite occur in association with galena and sphalerite as segregations around these sulfides or form rims of various morphologies. Complex iron oxides containing arsenic, antimony, and sulfur are widespread within the quartz matrix, occurring as intricate formations, collomorphic aggregates, and radial-acicular aggregates within the vein matrix.

### 3.4. Fluid-inclusion study

The fluid inclusions are predominantly represented by two-phase gas-liquid and vapor-enriched inclusions, the latter being rare. The inclusions are small, generally not exceeding 5 μm. Primary gas-liquid and vapor-enriched inclusions are typically isolated; however, the coexistence of both types was also observed. Only some of the fluid inclusions were available for measurements. Fluid inclusions in quartz from Stages I–II homogenize at temperatures ranging from 236 to 277 °C, with salinity varying from 1.6 to 2.6 wt.% (NaCl eq.). Fluid inclusions from the fahlore-gold-telluride-selenide-quartz assemblage yielded slightly lower temperatures, between 210 and 249 °C, with salinity varying from 0.5 to 1.7 wt.% (NaCl eq.) (**Table S5**).

## 4. Discussion

### 4.1. The mineral paragenetic sequence

According to documented mineral parageneses and the textural relationships of tennantite and tetrahedrite with other ore minerals, the following sequence of mineral formation is established for the Vilyuchinskoe ore occurrence (**Figure 4**).

Stage I. The early mineral assemblage is represented by discrete grains of weakly zoned fahlore minerals in quartz, which precipitated together with pyrite and chalcopyrite. Fahlores of this stage are characterized by a predominance of the tennantite with a gradual increase in Sb toward the marginal zones of the tennantite grains (**Figure 3g**). Stage II. The second mineral assemblage is characterized by the coeval precipitation of pyrite, sphalerite, and galena from the hydrothermal solution. In this mineral association, fahlore precipitated after the main sulfides (**Figure 4**). It commonly overgrows chalcopyrite, exhibits a complex internal texture, and is composed predominantly of the tetrahedrite component. Stage III. The final stage of mineralization is characterized by the crystallization of gold-bearing, tellurium-rich varieties of tetrahedrite and goldfieldite, silver tellurides (petzite, calaverite) and selenides (naumannite, clausthalite). This stage is marked by Te-rich fahlore varieties and goldfieldite, a feature typical of the late stages of hydrothermal system development. The appearance of calaverite, petzite, naumannite, and clausthalite is strictly confined to Stage III, where some of them occur as inclusions within Te-rich fahlore and goldfieldite. This textural relationship indicates that Au-Ag-Te and Ag-Pb-Se mineralization was coeval with the latest fahlore generation and postdates the main sulfide stage.

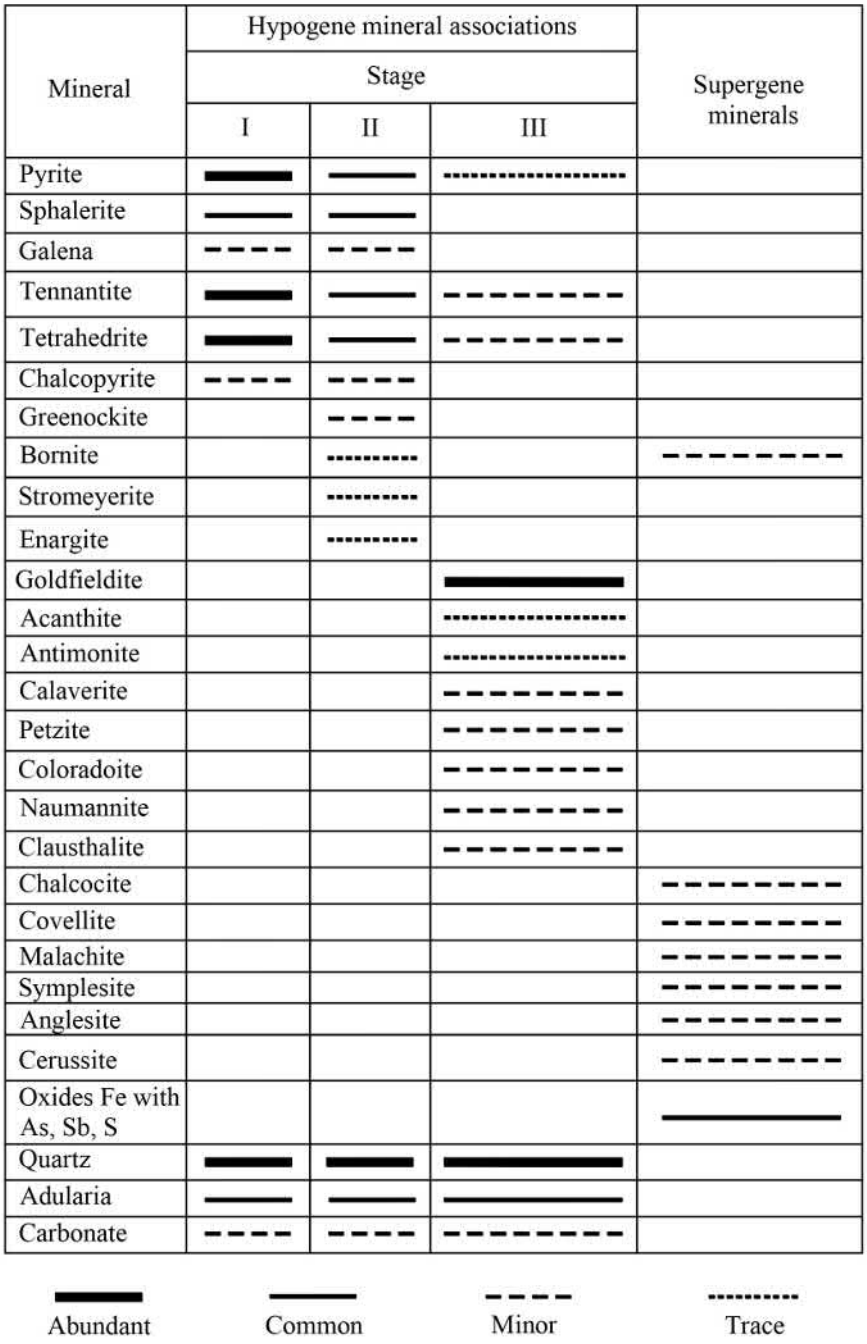



**Figure 4.** The paragenetic sequence of the minerals at the Vilyuchinskoe gold–silver ore occurrence.

## 4.2. Compositional trends of fahlore as a reflection of ore-forming fluid evolution

The plot of As against (Sb + Te + Bi) presented in **Figure 5a** displays a pronounced negative correlation, indicating that the principal substitution in the tetrahedral site is the heterovalent replacement of As by Sb, Te, and Bi. Stage I fahlore clusters in the upper-left field with high As (about 4.0 apfu) and low (Sb + Te + Bi) (below 1.5 apfu), reflecting early crystallization from an As-rich fluid. Stage II fahlore occupies an intermediate position, with decreasing As and increasing (Sb + Te + Bi), marking a transitional stage during which As was progressively

replaced by Sb, Te, and Bi. Stage III fahlore plots in the lower-right field with low As and high (Sb + Te + Bi), corresponding to Te-rich goldfieldite and its varieties. This shift reflects a change in fluid chemistry associated with an increase in Te and Se activity and a decrease in As activity that accompanied the late-stage precipitation of Au-Ag tellurides.

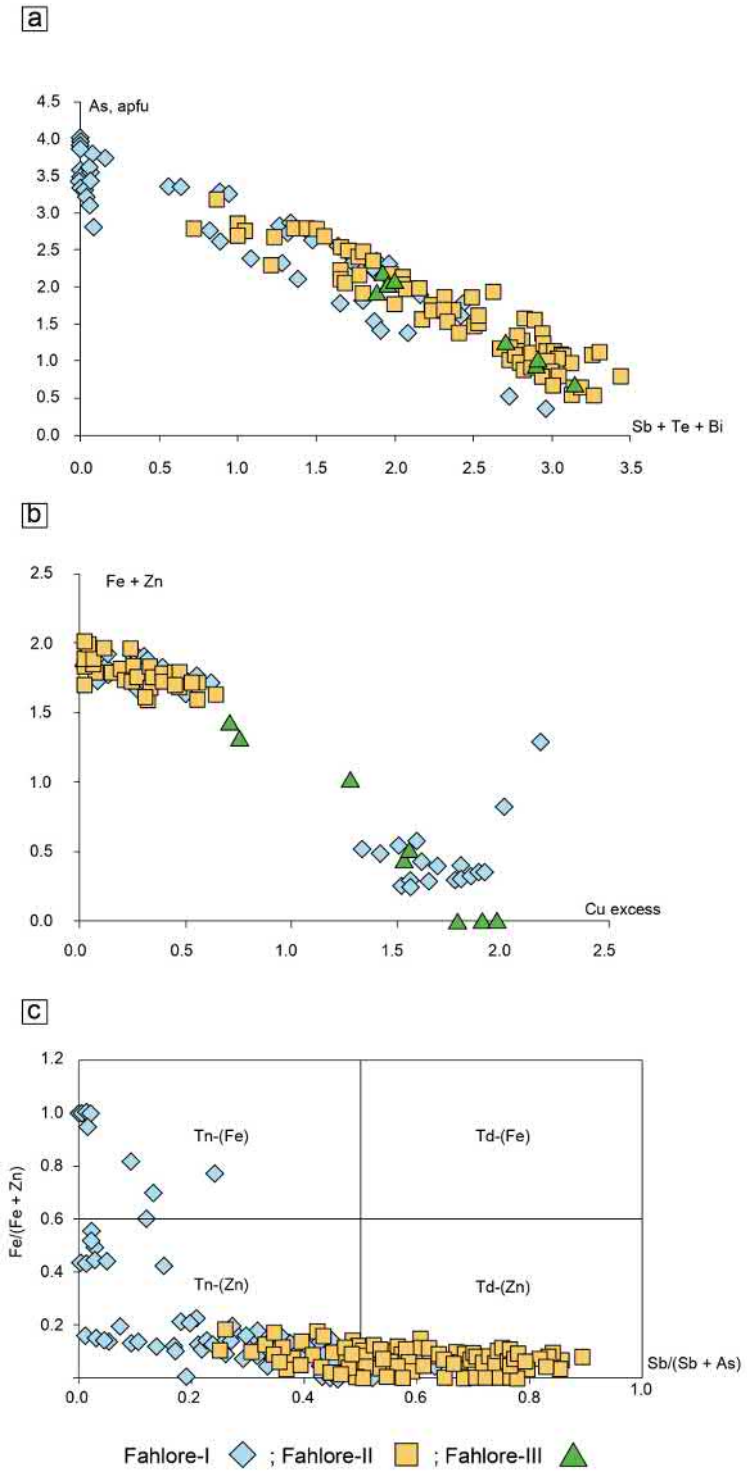



**Figure 5.** Compositional variations in fahlore from the Vilyuchinskoe ore occurrence: (**a**) As vs. (Sb + Te + Bi); (**b**) (Fe + Zn) vs. Cu excess, and (**c**) Fe/(Fe + Zn) vs. Sb/(Sb + As) diagrams for fahlore-I, II, III.

The plot of (Fe + Zn) versus Cu excess (**Figure 5b**) shows a negative correlation, indicating that Fe and Zn are progressively replaced by Cu excess. Stage I fahlore displays more scatter, with variable Cu excess and low (Fe + Zn), consistent with fluctuating fluid conditions during oscillatory growth. Stage II fahlore exhibits low Cu excess and high (Fe + Zn), indicating crystallization from a fluid with moderate oxygen fugacity. Stage III fahlore shows a gradual decrease in (Fe + Zn) along with an increase in Cu, which might be related to increasing oxygen and Te activity during Stage III (**Figure 6**). The Fe/(Fe + Zn) versus Sb/(Sb + As) plot (**Figure 5c**) shows a gentle compositional trend of fahlore from Zn-rich tennantite of Stage I to Zn-rich tetrahedrite of Stage II. The low Fe/(Fe + Zn) values (less than 0.5) are characteristic of an intermediate sulfidation state and are also an important distinguishing feature of a transition or subepithermal stage from a porphyry stage [21, 22]. The trend of fahlore from the Vilyuchinskoe ore occurrence coincides with those identified at the Peschanka and Nakhodka ore deposits, Russia and some others in China, which belong to transitional systems [21, 22].

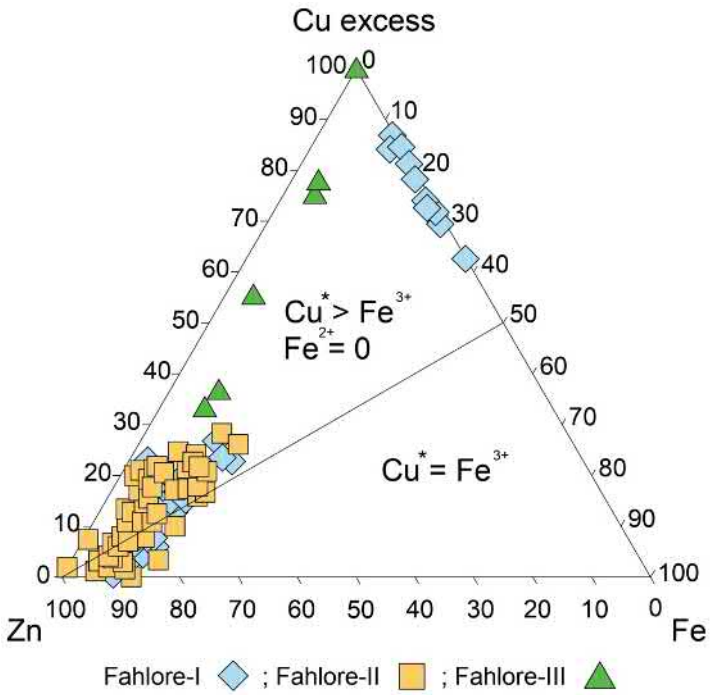



**Figure 6.** This base map is adapted from [22]: Cu* is defined as (Cu + Ag) − 10 for 12 metal atoms per formula unit, i.e., the amount of copper in excess. Compositions in the lower field satisfy Cu* = $Fe^{3+}$, where excess Cu is balanced by $Fe^{3+}$. Compositions in the upper field have Cu* > $Fe^{3+}$, indicating that excess Cu is not balanced by $Fe^{3+}$; consequently, $Cu^{2+}$ must be present and $Fe^{2+}$ absent.

It is known that copper-rich fahlore is precipitated from highly oxidizing fluids [23]. The Cu excess-Zn-Fe ternary diagram presented in **Figure 6** shows a systematic increase in Cu excess in fahlore from Stage I to Stage III, coupled with a decrease in the total (Fe + Zn) content. Some fahlore-I analyses plot on the Cu excess-Fe edge (i.e., the Zn = 0 line), indicating that early fahlore crystallized from fluids in which Zn was not incorporated, while Cu and Fe dominated the tetrahedral sites. The inferred oxygen fugacity ($fO_2$) therefore increases in the following order, Stage I < Stage II < Stage III, as constrained primarily by the increase in Cu excess and the concomitant decrease in (Fe + Zn). The predominance of Zn over Fe in most of the studied fahlore (Zn > Fe) is consistent with, and provides an additional indicator of these increasingly oxidizing conditions. Thus, the ore-forming fluid evolved under decreasing temperature and increasingly oxidizing conditions. Selenides occurring within the late paragenetic mineral association are also indicators of the higher $fO_2$ [13, 14].

A distinctive feature of the fahlore from the Vilyuchinskoe ore occurrence is the presence of rare and trace elements, particularly indium and bismuth. Indium is relatively rare in fahlore, and its concentrations are generally low. However, anomalously high indium contents, up to 6.5 wt.%, have been reported in fahlore from the epithermal Pefka deposit (Greece) [24]. In the studied fahlore, indium is confined exclusively to first-generation tennantites enriched in As and depleted in Sb, Zn, and Ag. The In content in these tennantites ranges from 1.34 to 2.26 wt.%, which generally exceeds the values known from the Morococha deposit, Peru [25], and the Capillitas deposit, Argentina [26]. A positive correlation of In with As and Fe and a negative correlation with Sb, Zn, and Ag are observed. The oscillatory zoning of the first generation probably records As/Sb fluctuations, with In concentrating in the As-dominant zones. It should also be taken into account that, when sphalerite is present, indium preferentially enters its structure rather than that of fahlore, which is due to their crystal-chemical characteristics. Sphalerite occurs in Stage I with a content of FeS of 1.51 mol.% (0.75 wt.%). A theoretical study [27] confirms that the presence of Fe in sphalerite also stabilizes indium incorporation. In the studied samples, however, indium is hosted by Cd-bearing sphalerite that is free of Fe. This indicates an independent mechanism of indium input into the fluid, possibly related to the episodic influx of this element. The presence of minor amounts of Cu, Ag, and Sb in sphalerite may be due to either isomorphic substitution or micro-inclusions of chalcopyrite and fahlore [28]. However, indium, which forms its own zones, most likely enters the sphalerite structure through isomorphous substitution of Zn [27, 29]. The lower indium concentrations in fahlore compared with sphalerite are probably due to earlier crystallization of sphalerite, which captured most of the indium from the fluid. This is consistent with global statistics, according to which sphalerite is the principal concentrator of indium in hydrothermal systems [30].

Bismuth, like indium, is also a trace element in fahlore. In the studied fahlore, bismuth contents reach up to 5.11 wt.%, which is much lower compared with other deposits worldwide [31]. In the fahlore of the Vilyuchinskoe ore occurrence, bismuth is concentrated in minor amounts in tennantites of the first generation. Higher bismuth contents are characteristic of tetrahedrite of the second generation. Thus, Bi activity increased in the late ore-forming fluids. Experimental data indicate that the solubility of Bi in tetrahedrite-tennantite grains is 0.8 apfu at 350 °C and 1.0 apfu at 450–520 °C, regardless of the Sb/As ratio. Moreover, Bi solubility increases with increasing sulfur fugacity and, correspondingly, decreases as sulfur fugacity decreases [32]. The maximum bismuth concentrations in the studied fahlore are 2.17–5.11 wt.%, corresponding to approximately 0.2–0.4 apfu. These values are significantly below the experimental solubility limit and are consistent with fluid inclusion data. This indicates that the system did not attain saturation with respect to bismuth, and its concentration was controlled mainly by the activity of Bi in the fluid rather than by the solubility limit in the structure.

The majority of the studied fahlore display heterogeneous internal textures, mainly due to the uneven distribution of arsenic and antimony. Two types of zoning are recognized: oscillatory zoning with alternating changes in antimony and arsenic contents in tennantite of the first generation, and complex mosaic-block zoning in fahlore of the second generation. The oscillatory zoning indicates deposition of early fahlore generations under conditions of dynamic changes in the physicochemical parameters of the ore-forming environment caused by boiling or mixing of hydrothermal fluids. Evidence for boiling of hydrothermal fluids is further provided by the coexistence of liquid-rich and vapor-rich inclusions. The second-generation fahlore, which predominantly replaces early sulfides, was probably deposited from evolved lower-temperature fluids, which controlled the solubility of the end members of the solid solution.

## 4.3. Physicochemical conditions of ore formation

The three stages identified in this study correspond to different physicochemical parameters of the ore-forming fluid. The first two mineral assemblages are characterized by similar of sulfides and sulfosalts, including minerals typical of intermediate-sulfidation (IS) epithermal systems such as tennantite-tetrahedrite series minerals, pyrite, chalcopyrite, and sphalerite with trace amounts of greenockite and enargite [33]. Therefore, it may be suggested that these stages formed under conditions of relatively high sulfur fugacity. Using fluid inclusion temperature data and FeS contents of sphalerite, the sulfur fugacities were calculated for Stage I and Stage II (**Figure 7**). The sulfur fugacity ($fS_2$) was calculated using the stability fields of coexisting sulfides (pyrite-pyrrhotite, sphalerite-pyrite) following the method of [34]. The precipitation of the initial sulfide mineralization began at log $fS_2$ of ~−8.58 (**Figure 7**), followed by a decrease to ~−13.15, as indicated by the precipitation of Fe-poor sphalerite, the replacement of chalcopyrite by tennantite and tetrahedrite, and a gradual decrease in temperature. Both mineral assemblages fall within the sulfidation transition zone, which confirms the above conclusion regarding an intermediate-sulfidation state based on fahlore data. The appearance of tellurides in Stage III indicates a sharp increase in $f_{Te2}$. According to [35, 36], calaverite precipitates at high Te fugacity, near the stability boundary of the native gold-calaverite assemblage. In the present study, gold was found as Au-Ag tellurides. Thus, we suppose that tellurides of Stage III along with goldfieldites and selenides, precipitated at log $fTe_2$ values above −10; the native gold (Au)-calaverite ($AuTe_2$) reaction occurs at temperatures of 256 °C.

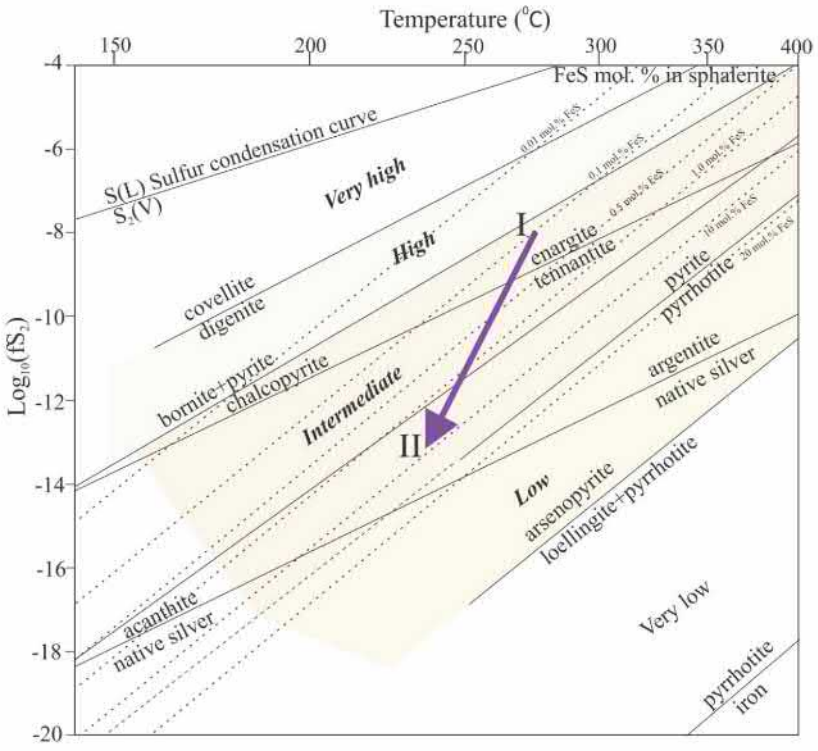



**Figure 7.** Temperature-sulfur fugacity diagram, showing deposition of the sulfides and sulfosalts during Stages I and II of the mineral formation at the Vilyuchinskoe ore occurrence with relative sulfidation states of hydrothermal fluids in porphyry deposits and epithermal ore mineral stability fields (modified from [37]). The purple arrow (I → II) indicates the evolutionary trend of the ore-forming fluid from Stage I to Stage II, reflecting a decrease in temperature and sulfur fugacity. The dotted lines represent the contours of FeS mol.% in sphalerite (from 0.01 to 20 mol.% FeS). The solid lines mark the equilibrium boundaries of the mineral buffer reactions (e.g., acanthite/native silver and argentite/native silver).

Fahlores are important carriers of Ag, as evidenced by the high Ag contents in tetrahedrite varieties (up to 0.67 apfu). However, no direct evidence for the isomorphous incorporation of Au into the structure was found in the studied samples; the bulk of gold appears to be hosted by Au-Ag tellurides enclosed within fahlore-III, with associated Ag and Pb selenides that do not contain Au. This suggests that fahlores act as indicators of conditions favorable for the precipitation of Au-Ag tellurides: high $fTe_2$ and low $fS_2$ typical of the late low-temperature stage. Furthermore, the presence of telluride inclusions exclusively within fahlore-III, rather than in earlier generations, indicates that these minerals crystallized simultaneously with, or immediately prior to, telluride deposition, which is in agreement with experimental data on the stability of gold tellurides at temperatures below 250 °C [36].

The first K-Ar ages for ore mineralization at the Vilyuchinskoe ore occurrence were reported by Okrugin [38] and Takahashi et al. [39], yielding ages of 5.3 ± 0.3 and 5.1 ± 0.3 Ma, respectively. In later studies [15], based on dating of vein adularia, a younger age of ore mineralization was established with a value of 1.4 ± 0.3 Ma. New dating of adularia from the Regina vein zone yielded ages defining two distinct intervals 4.8 ± 0.3 Ma and 1.18 ± 0.18 Ma and 1.49 ± 0.19 Ma. These may be attributed to two distinct hydrothermal episodes: Pliocene (~5 Ma) and Early Pleistocene (~1.3 Ma). However, all obtained ages fall within the range of previously published values (5.3 ± 0.3, 5.1 ± 0.3 and 1.4 ± 0.3 Ma). Thus, this supports our dating and indicates at least two major episodes of fluid activity: 5.3–4.8 and 1.49–1.18 Ma. The 5.3–4.8 Ma interval coincides with a change in the Kamchatka subduction regime during the Pliocene, which triggered tectonic reorganization and magmatic activation along the eastern margin of the peninsula [40, 41]. Two obtained Early Pleistocene dates (1.49 ± 0.19 and 1.18 ± 0.18 Ma) and one previously published date (1.4 ± 0.3 Ma) correspond to a stage of subsequent tectonic reactivation, which renewed fluid flow along pre-existing faults but did not produce fundamentally new structures. Although we cannot precisely determine the age of each stage, we can state that the formation of vein bodies at the Vilyuchinskoe ore occurrence began no earlier than 5.3 Ma and continued until 1.18 ± 0.18 Ma. Similar age characteristics have also been established for other gold–silver deposits in Kamchatka [42, 43], Japan [44], and Indonesia [45].

## 5. Conclusions

The ore mineralization at the Vilyuchinskoe ore occurrence, comprising sulfosalts, sulfides, tellurides, and selenides, developed in three stages. Fahlores occur throughout all three stages and are the principal carriers of In, Bi, and Ag. The tetrahedrite-group minerals evolved from early tennantite and tetrahedrite (Stage I) through tetrahedrite-dominated varieties (Stage II) to Te-rich goldfieldite (Stage III), recording an increase in Cu excess (from ~9.82 to 12.00 apfu), a decrease in (Fe + Zn), and As→Sb→Te substitution. All studied fahlores are zincian varieties with low Fe contents. The compositional changes in fahlores and inner zoning indicate that Stages I–II fahlores formed under high sulfur fugacity from hydrothermal fluids at 236–277 °C with salinity of 1.6–2.6 wt.% NaCl eq. The late fahlores, represented by goldfieldite, formed at lower sulfur fugacity and higher Te and Se activity, accompanied by a decrease in temperature and fluid salinity (210–249 °C, 0.5–1.7 wt.% NaCl eq.). The compositional trend from Zn-rich tennantite of Stage I to Zn-rich tetrahedrite of Stage II is typical of intermediate-sulfidation (IS) systems and has been documented in IS deposits elsewhere. The Vilyuchinskoe ore occurrence is classified as a transitional sub-epithermal intermediate-sulfidation system. New geochronological data indicate at least two pulses of hydrothermal activity, in the Pliocene (~5 Ma) and Early Pleistocene (~1.3 Ma).

## Acknowledgments

The authors thank the staff of the Laboratory of Volcanogenic Ore Formation for their help with sample preparation. The authors acknowledge the use of the AI tool DeepSeek-V4 for language editing. The tool was applied to enhance clarity and scholarly tone, and all edits were carefully reviewed and validated by the authors to ensure accuracy, compliance with academic standards, and research integrity. The authors fully support Academia.edu Journals' adherence to COPE guidelines on AI in publication ethics and confirm that this use has been managed responsibly and ethically.

## Funding

This research received no external funding.

## Author contributions

Conceptualization, E.D.S. and I.V.V.; methodology, V.V.K.; validation, E.D.S.; formal analysis, K.O.S., D.A.Y. and V.A.L.; investigation, E.D.S., K.O.S., D.A.Y., O.R.R. and V.V.K.; writing—original draft preparation, E.D.S., K.O.S. and D.A.Y.; writing—review and editing, E.D.S., K.O.S., D.A.Y., O.R.R., V.V.K., V.A.L. and I.V.V. All authors have read and agreed to the published version of the manuscript.

## Conflict of interest

The authors declare that they have no competing interests.

## Data availability statement

All data supporting the findings of this publication are available within this article and its supplementary materials.

## Supplementary materials

The supplementary materials are available at https://doi.org/10.20935/AcadEPS8589.

## Publisher's note

Academia.edu Journals stays neutral regarding jurisdictional claims in published maps and institutional affiliations. All claims expressed in this article are solely those of the authors and do not necessarily represent those of their affiliated organizations, or those of the publisher, the editors, and the reviewers. Any product that may be evaluated in this article, or claim that may be made by its manufacturer, is not guaranteed or endorsed by the publisher.

## Copyright

© 2026 copyright by the authors. This article is an open access article distributed under the terms and conditions of the Creative Commons Attribution (CC BY) license.

## References

1. Vassileva RD, Atanassova R, Kouzmanov K. Tennantite-tetrahedrite series from the Madan Pb-Zn deposits, Central Rhodopes, Bulgaria. Mineral Petrol. 2014; 108 (4): 515–31. doi: 10.1007/s00710-013-0316-0
2. Kase K. Tellurian tennantite from the Besshi-type deposits in the Sambagawa metamorphic belt, Japan. Can Mineral. 1986; 24 (2): 399–404.
3. Spiridonov EM, Ivanova YN, Yapaskurt VO. Selenium-bearing goldfieldite and fischesserite $AuAg_3Se_2$-petzite $AuAg_3Te_2$ solid solutions in ores of the Ozernovskoe volcanogenic deposit (Kamchatka). Dokl Earth Sci. 2014; 458 (1): 1139–42. doi: 10.1134/S1028334X14090219
4. Krismer M, Vavtar F, Tropper P, Kaindl R, Sartory B. The chemical composition of tetrahedrite-tennantite ores from the prehistoric and historic Schwaz and Brixlegg mining areas (North Tyrol, Austria). Eur J Mineral. 2011; 23 (6): 925–36. doi: 10.1127/0935-1221/2011/0023-2137
5. Wei D, Xia Y, Steadman JA, Xie Z, Liu X, Tan Q, et al. Tennantite-tetrahedrite-series minerals and related pyrite in the Nibao Carlin-type gold deposit, Guizhou, SW China. Minerals. 2021; 11 (1): 2. doi: 10.3390/min11010002
6. Antal B. Tennantite from the vein Mayer, Baňa Mária deposit in Rožňava, Spišsko-gemerské rudohorie Mts. Slovak Geol Mag. 2002; 8 (3–4): 195–204.
7. Biagioni C, George LL, Cook NJ, Makovicky E, Moëlo Y, Pasero M, et al. The tetrahedrite group: nomenclature and classification. Am Mineral. 2020; 105 (1): 109–22. doi: 10.2138/am-2020-7128
8. Makovicky E, Karanović L, Poleti D, Balić-Žunić T, Paar WH. Crystal structure of copper-rich unsubstituted tennantite, $Cu_{12.5}As_4S_{13}$. Can Mineral. 2005; 43 (2): 679–88. doi: 10.2113/gscanmin.43.2.679
9. Biagioni C, Sejkora J, Moëlo Y, Marcoux E, Mauro D, Dolníček Z. Tennantite-(Cu), $Cu_{12}As_4S_{13}$, from Layo, Arequipa Department, Peru: a new addition to the tetrahedrite-group minerals. Mineral Mag. 2022; 86 (2): 331–9. doi: 10.1180/mgm.2022.26
10. Kovalenker VA, Plotinskaya OY. Te and Se mineralogy of Ozernovskoe and Prasolovskoe epithermal gold deposits, Kuril–Kamchatka volcanic belt. In: Cook NJ, Bonev IK, editors. Proceedings of the IGCP Project 486 2005 Field Workshop Au-Ag-Te-Se Deposits; 14–19 September 2005; Kiten, Bulgaria. Sofia, Bulgaria: Bulgarian Academy of Sciences; 2005. p. 118–23.
11. Spiridonov EM, Okrugin VM. Selenious goldfieldite—a new variety of fahlores. Dokl Akad Nauk SSSR. 1985; 280 (2): 476–8.
12. Okrugin VM, Shishkanova KO, Philosophova TM. New data on ores from the Vilyuchinskoe Au-Ag polymetallic ore occurrence, Southern Kamchatka. Ores Met. 2017; 1: 40–54.
13. Kudaeva SS, Kozlov VV, Skilskaya ED, Sergeeva AV, Tolstykh ND, Shkilev IA. New type of gold-bearing mineralization at the Ozernovskoe Au-Te-Se epithermal deposit (Central Kamchatka, Russia). Geol Ore Depos. 2024; 66 (5): 547–69. doi: 10.1134/S1075701524600427
14. Tolstykh ND, Shapovalova MO, Chubarov VM. Evolution of composition of tetrahedrite and enargite sulfosalts in the Maletoyvayam Au-Ag deposit (Kamchatka). Russ Geol Geophys. 2025; 66 (5): 613–29. doi: 10.2113/RGG20244818

15. Shishkanova KO. New data on fahlores of the Vilyuchinskoe ore occurrence (Southern Kamchatka). Bull Kamchatka Reg Assoc «Educ-Sci Cent» Earth Sci. 2025; 68 (4): 50–8. doi: 10.31431/1816-5524-2025-4-68-50-58
16. Petrenko ID. Gold-silver formation of Kamchatka. Petropavlovsk-Kamchatsky, Russia: Saint Petersburg Cartographic Factory of VSEGEI; 1999.
17. Takahashi R, Matsueda H, Okrugin VM. Hydrothermal gold mineralization at the Rodnikovoe deposit in South Kamchatka, Russia. Resour Geol. 2002; 52 (4): 359–69. doi: 10.1111/j.1751-3928.2002.tb00146.x
18. Lezin VI, Bondar VA, Prozorovsky VA. Report on the results of preliminary exploration of the central part of the Rodnikovoe deposit for 1984–1988 years. Petropavlovsk-Kamchatsky, Russia: Central Kamchatka Geological Expedition; 1988.
19. Bodnar RJ. Revised equation and table for determining the freezing point depression of $H_2O$-NaCl solutions. Geochim Cosmochim Acta. 1993; 57 (3): 683–4. doi: 10.1016/0016-7037(93)90378-A
20. Takahashi R, Matsueda H, Okrugin VM, Ono S. Polymetallic and Au-Ag mineralizations at the Mutnovskoe Deposit in South Kamchatka, Russia. Resour Geol. 2006; 56 (2): 141–56. doi: 10.1111/j.1751-3928.2006.tb00275.x
21. Marushchenko LI, Baksheev IA, Nagornaya EV, Chitalin AF, Nikolaev YN, Vlasov EA. Compositional evolution of the tetrahedrite solid solution in porphyry-epithermal system: a case study of the Baimka Cu-Mo-Au trend, Chukchi Peninsula, Russia. Ore Geol Rev. 2018; 103: 21–37. doi: 10.1016/j.oregeorev.2017.01.018
22. Long H, Liu W, Chen J, Qiu J, Li J, Chen H, et al. Compositional evolution of fahlores in the Zijinshan porphyry-epithermal Cu-Au-Mo-Ag ore field, China, and implications for prospecting. Minerals. 2025; 15 (4): 362. doi: 10.3390/min15040362
23. Spiridonov EM, Maleev M, Kovachev V, Kulikova I, Nazmova G, Filimonov S. Minerals of fahlore group: indicators of ore genesis. In: Proceedings of the Jubilee International Conference Bulgarian Geological Society 80th Anniversary; 17–18 November 2005; Sofia, Bulgaria. Sofia, Bulgaria: Bulgarian Geological Society; 2005. p. 79–82.
24. Voudouris P, Repstock A, Spry PG, Frenzel M, Mavrogonatos C, Keith M, et al. Physicochemical constraints on indium-, tin-, germanium-, gallium-, gold-, and tellurium-bearing mineralizations in the Pefka and St Philippos polymetallic vein- and breccia-type deposits, Greece. Ore Geol Rev. 2022; 140: 104348. doi: 10.1016/j.oregeorev.2021.104348
25. Benites D, Torró L, Vallance J, Laurent O, Valverde PE, Kouzmanov K, et al. Distribution of indium, germanium, gallium and other minor and trace elements in polymetallic ores from a porphyry system: the Morococha district, Peru. Ore Geol Rev. 2021; 136: 104236. doi: 10.1016/j.oregeorev.2021.104236
26. Márquez-Zavalía MF, Vymazalová A, Galliski MA, Watanabe Y, Murakami H. Indium-bearing paragenesis from the Nueva Esperanza and Restauradora veins, Capillitas mine, Argentina. J Geosci. 2020; 65 (2): 97–109. doi: 10.3190/jgeosci.304
27. Yang X, Li Y, Chen J. DFT study of the occurrence state of In and the correlation of In and Fe in sphalerite. Miner Eng. 2022; 183: 107596. doi: 10.1016/j.mineng.2022.107596
28. Kumar AA, Sanislav IV, Cathey HE, Dirks PH. Geochemistry of indium in magmatic-hydrothermal tin and sulfide deposits of the Herberton Mineral Field, Australia. Miner Depos. 2023; 58 (7): 1297–316. doi: 10.1007/s00126-023-01179-7
29. Xiao F, He Z, Zheng Y, Xiong S, Cheng Q. A DFT study on mechanisms of indium adsorption on sphalerite (100), (110), and (111) surfaces: implications for critical metal mineralization. Ore Geol Rev. 2025; 181: 106572. doi: 10.1016/j.oregeorev.2025.106572

30. Mejías OC, Parbhakar-Fox A, Jackson L, Valenta R, Townley B. Indium in ore deposits and mine waste environments: geochemistry, mineralogy, and opportunities for recovery. J Geochem Explor. 2023; 255: 107312. doi: 10.1016/j.gexplo.2023.107312
31. Sejkora J, Biagioni C, Dolníček Z, Velebil D, Škácha P. Annivite-(Zn), $Cu_6(Cu_4Zn_2)\Sigma_6Bi_4S_{13}$, from the Jáchymov ore district, Czech Republic: the first Bi-dominant member of the tetrahedrite group. Mineral Mag. 2025; 89 (1): 102–12. doi: 10.1180/mgm.2024.54
32. Klünder MH, Karup-Møller S, Makovicky E. Exploratory studies on substitutions in the tetrahedrite-tennantite solid solution series part III. The solubility of bismuth in tetrahedrite-tennantite containing iron and zinc. Neues Jahrb Mineral Monatshefte. 2003; 2003 (4): 153–75. doi: 10.1127/0028-3649/2003/2003-0153
33. Hedenquist JW, Arribas AR, Gonzalez-Urien E. Exploration for epithermal gold deposits. In: Hagemann SG, Brown PE, editors. Gold in 2000. Littleton, CO, USA: Society of Economic Geologists; 2000. p. 245–77. doi: 10.5382/Rev.13.07
34. Barton PB Jr, Skinner BJ. Sulfide mineral stabilities. In: Barnes HL, editor. Geochemistry of hydrothermal ore deposits. 2nd ed. New York, NY, USA: John Wiley & Sons; 1979. p. 278–403.
35. Afifi AM, Kelly WC, Essene EJ. Phase relations among tellurides, sulfides, and oxides: I. Thermochemical data and calculated equilibria. Econ Geol. 1988; 83 (2): 377–94. doi: 10.2113/gsecongeo.83.2.377
36. Afifi AM, Kelly WC, Essene EJ. Phase relations among tellurides, sulfides, and oxides: II. Applications to telluride-bearing ore deposits. Econ Geol. 1988; 83 (2): 395–404. doi: 10.2113/gsecongeo.83.2.395
37. Einaudi MT, Hedenquist JW, Inan EE. Sulfidation state of fluids in active and extinct hydrothermal systems: transitions from porphyry to epithermal environments. In: Simmons SF, Graham I, editors. Volcanic, geothermal and ore-forming fluids: rulers and witnesses of processes within the Earth. Littleton, CO, USA: Society of Economic Geologists; 2003. p. 285–313. doi: 10.5382/sp.10.15
38. Okrugin VM. On the age and genesis of epithermal deposits in the continent-ocean transition zone (north-western Pacific). In: Modern volcanism and related processes. Petropavlovsk-Kamchatsky, Russia: KSPU; 2002. p. 56–7.
39. Takahashi R, Matsueda H, Okrugin VM, Shikazono N, Ono S, Imai A, et al. Ore-forming ages and sulfur isotope study of hydrothermal deposits in Kamchatka, Russia. Resour Geol. 2013; 63 (2): 210–23. doi: 10.1111/rge.12005
40. Khanchuk AI, Grebennikov AV. Late Miocene-Pliocene transform margin of Kamchatka. Pac Geol. 2021; 40 (5): 3–15. doi: 10.30911/0207-4028-2021-40-5-3-15
41. Yablokova DA, Skilskaya ED, Vikentyev IV, Boiko AU, Lebedev VA. Age of the epithermal Rodnikovoe Au–Ag deposit (South Kamchatka). Dokl Earth Sci. 2026; 529: 3. doi: 10.1134/S1028334X26600957
42. Schweigert PE, Bukhanova DS, Zhegunov PS. K–Ar ages of adularia-quartz veins from the Tutkhlivayam ore occurrence (Kamchatka). Russ J Earth Sci. 2026; 26: ES3010. doi: 10.2205/2026es001143
43. Tolstykh ND, Shapovalova MO, Podlipsky M. Au-Ag-Se-Te-S mineralization in the Maletoyvayam high-sulfidation epithermal deposit, Kamchatka Peninsula. Minerals. 2023; 13 (3): 420. doi: 10.3390/min13030420
44. Enatsu M, Shimoji Y, Koike K, Shirose Y, Watanabe Y. Ore geochemical composition characterization of hydrothermal deposits throughout the Japanese Islands: interpreting spatial and temporal metallogeny. Ore Geol Rev. 2025; 187: 106979. doi: 10.1016/j.oregeorev.2025.106979
45. Titisari AD, Phillips D, Warmada IW, Hartono, Idrus A. $^{40}Ar/^{39}Ar$ geochronology of the Pongkor low sulfidation epithermal gold mineralisation, West Java, Indonesia. Ore Geol Rev. 2020; 119: 103341. doi: 10.1016/j.oregeorev.2020.103341